Article:

Wang, K, Ma, Y, Howlett, PR et al. (2 more authors) (2022) New Unsaturated Dynamic Porosity Hydromechanical Coupled Model and Experimental Validation. International Journal of Geomechanics, 22 (10). 04022171. ISSN 1532-3641

https://doi.org/10.1061/(asce)gm.1943-5622.0002545

New unsaturated dynamic porosity hydro-mechanical coupled model and experimental validation

Kai Wang[1]; Yue Ma[2]; Paul R. Howlett[3]; Aizhong Ding, Ph.D.[4*]; Xiao - Hui Chen, Ph.D.[5*]

[1]College of Water Sciences, Beijing Normal University, Beijing, 100875, China, E-mail address: wangkaik@mail.bnu.edu.cn

[2]School of Civil Engineering, University of Leeds, Leeds, LS2 9JT, UK, E-mail address: cnym@leeds.ac.uk

[3]School of Civil Engineering, University of Leeds, Leeds, LS2 9JT, UK, E-mail address: cnprh@leeds.ac.uk

[4]College of Water Sciences, Beijing Normal University, Beijing, 100875, China, E-mail address: ading@bnu.edu.cn

[5]School of Civil Engineering, University of Leeds, Leeds, LS2 9JT, UK, E-mail address: X.Chen@leeds.ac.uk

Abstract

Constitutive coupled modeling has developed rapidly in recent decades, with numerous new models published. However, few models consider dynamic porosity, and experimental validation of such a model remains a challenge due to multiple variables. In this study, a new constitutive model for unsaturated soil with dynamic porosity was developed and validated using test data from two experimental studies that yielded good results (relative average error AVRE = 0.8631-1.3046, R^2 = 0.9028–0.9981). The sensitivity of the model to the four primary parameters was analyzed to investigate the influence of model properties on the hydraulic and mechanical behavior. Results show that the calculation of volumetric strain is most sensitive to Young's modulus (E), while the calculation of specific water volume is most sensitive to permeability (k). Also, the sensitivity of the parameters changes with their value. Modeled results show that the porosity change significantly affects both hydraulic and mechanical behavior, even when soil undergoes relatively low deformation. Relative calculation error decreases notably after porosity change is considered (44.9% and 35.2% improvement in two different calculations). This study also finds that dynamic porosity affects the deformation energy of solids.

Keywords: Biot's theory; Mixture coupling theory; Unsaturated soil; Dynamic porosity; Model validation; Parameter sensitivity

Introduction

Since Terzaghi developed the one-dimensional consolidation theory of saturated soil (Terzaghi 1943), research into coupled hydro-mechanical models has been an important topic in many engineering applications. Safety analysis for nuclear waste disposal must evaluate the long-term deformation of barrier rock and potential environmental risk to the host rock and local groundwater (Félix et al. 1996, Charlier et al. 2013, Schwartz 2018). The prediction of fluid inflow into tunnels as well as deformation at dams requires an understanding of the coupled relationships between rock displacement, pore moisture and water flow (Chen et al. 2016, Zhang et al. 2020). Hydro−mechanical coupling is required for studies of rock slope deformation induced by precipitation infiltration (Masoudian et al. 2019) and research into groundwater flow in shale rock and hydraulic fracturing during shale gas exploitation (Lisjak et al. 2017). Many cases of coupled hydro-mechanical behavior occur in an unsaturated zone, which highlights the importance of studies of coupled hydro-mechanical models in unsaturated media.

Two approaches can be used to derive most of the coupling theory of hydro-mechanical behavior: the mechanics approach and the mixture approach. The mechanics approach is based primarily on the work of Terzaghi (Terzaghi 1943) and Biot's theory (Biot 1941, Biot 1962). Many models have been developed using this approach, including unsaturated hydro-mechanical models (Sanavia et al. 2002, Li and Yang 2018), large-strain hydro-mechanical models (Meroi et al. 1995), multiphase flow models (Edip et al. 2018), and coupled thermo-hydro-mechanical-chemical models (Li et al. 2006, Seetharam et al. 2007). This approach has found to be useful when developing new models for specific applications (e.g., introducing formulations of other fields to the constitutive model) and has supported many practical areas of geomechanics and engineering. However, this approach lacks a systemic, self-developing linkage between different fields, making it difficult to use to build a unified coupling theory for porous media (Chen et al. 2016).

A different approach, mixture theory, originated from biological tissue engineering and was developed by Truesdell (Truesdell 1962). Mixture theory is based on non-equilibrium thermodynamics but has yet to describe the coupled interactions of different phases.

Recently, mixture coupling theory, which was previously called modified mixture theory, was developed by Heidug and Wong (Heidug and Wong 1996), has been used to build more advanced coupled models in geomechanics and geophysics (Chen and Hicks 2013a, Chen et al. 2013b, Chen et al. 2016, Ma et al. 2021). Instead of discriminating between solid and fluid phases, as the previous mixture theory does, mixture coupling theory treats the fluid-infiltrated system as a single continuum material. Mixture coupling theory builds a unified theory of multifield behaviors in soil and rocks using entropy production as a single driving force.

Mixture coupling theory has demonstrated marked advantages in developing systemic multifield coupling models in both unsaturated and saturated media. Chemical osmosis, including dual-chemical osmosis, and thermal osmotic processes were added into the hydro-mechanical-chemical model and the hydro-mechanical-thermal model (Chen and Hicks 2013a, Chen et al. 2018). To date, there has been little experimental validation of mixture coupling theory, primarily due to its recent application in geotechnology. Despite understanding the parameters of unsaturated hydro-mechanical coupling, the parameterization of models with material properties is currently inadequate. Some parameters are difficult to determine, and more effort is required to understand the sensitivity of the model results to different parameters.

In this study, a new constitutive model for unsaturated soil considering dynamic porosity is developed and validated using experimental data, and the sensitivity of hydraulic and mechanical behaviors to different parameters is evaluated. The new model is compared with a previous model that ignores porosity change. The deformation energy was studied to describe hydro-mechanical coupling behavior in more detail.

This study provides additional support for the development of the theoretical framework of mixture coupling theory in the field of geotechnics, develops a new coupled model considering porosity change, and provides a benchmark for model calibration and evaluation, particularly for sensitivity analysis. The proposed model exhibits marked potential for characterizing hydro-mechanical coupling behavior under nonnegligible porosity changes.

Theory

Basic unsaturated hydro-mechanical coupled governing equations

This paper is based on the coupled unsaturated hydro-mechanical (UHM) model for soil, which is based on mixture coupling theory (Chen and Hicks 2011), and provides a critical step forward by considering dynamic porosity and analyzing deformation energy. To completely introduce the theory upon which this study is based, the basic equation for the UHM coupled model is introduced as follows below.

1. Mechanical equation

The final governing field equation for the solid phase can be written as (Chen and Hicks 2011):

$$\left(K-\frac{2G}{3}\right)\frac{\partial^2 \dot{d}_k}{\partial x_k \partial x_i}+G\left(\frac{\partial^2 \dot{d}_i}{\partial x_j \partial x_j}+\frac{\partial^2 \dot{d}_j}{\partial x_i \partial x_j}\right)-\zeta\nabla\left[\left(S_w+\frac{C_s}{\upsilon}p^w\right)\dot{p}^w\right]=0 \qquad (1)$$

where G is the shear modulus; K is the bulk modulus; d is the displacement; ζ is Biot's consolidation coefficient, which is defined as $\zeta=1-(K/K_s)$, where K_s is the bulk modulus of the solid matrix); υ is the porosity; S_w is the saturation of pore water; p^w is the porewater pressure; and C_s is the specific moisture content, which is defined as $C_s=\upsilon\frac{\partial S_w}{\partial p_w}$) (Lewis et al. 1987).

Normally, C_s is small and is assumed to be zero for the convenience of calculation; thus, Equation (1) becomes:

$$\left(K-\frac{2G}{3}\right)\frac{\partial^2 \dot{d}_k}{\partial x_k \partial x_i}+G\left(\frac{\partial^2 \dot{d}_i}{\partial x_j \partial x_j}+\frac{\partial^2 \dot{d}_j}{\partial x_i \partial x_j}\right)-\zeta S_w\nabla \dot{p}^w=0 \qquad (2)$$

2. Hydraulic equation

The final governing field equation for the porewater can be written as (Chen and Hicks 2011):

$$S_w\zeta\dot{d}-\frac{k_{rw}k}{v}(\nabla^2 p^w)+(C_s+\upsilon\frac{S_w}{K_w})\frac{\partial p^w}{\partial t}+S_wQ(S_w+\frac{C_s}{\upsilon}p^w)\frac{\partial p^w}{\partial t}=0 \qquad (3)$$

where k is the permeability; k_{rw} is the relative permeability; v is the dynamic viscosity; K_w is the bulk modulus of water; and Q is the void compressibility, which is defined as $Q=(1/K_s)(\xi-\upsilon)$.

Normally, K_s is large compared to K_w (Alonso and Alcoverro 1999b), Q can be assumed to be zero, and thus, Equation (3) becomes:

$$S_w \zeta \nabla \cdot \dot{d} - \frac{k_{rw} k}{v}\left(\nabla^2 p^w\right) + S_w \upsilon q \frac{\partial p^w}{\partial t} = 0 \quad (4)$$

where $q = \frac{1}{K_w}$ is the poroelastic storage.

A key assumption of Equations (2) and (4) is that the porosity is constant, which is not validated in observations (Stormont and Daemen 1992) and is thus the primary focus of this study.

Unsaturated hydro-mechanical coupled governing equations with dynamic porosity

In the absence of chemical influence, a porosity function can be obtained based on mixture coupling theory (Chen and Hicks 2013a). This function will be incorporated in the coupled model:

$$\dot{\upsilon} = \zeta \dot{\varepsilon}_{ii} + Q \dot{p}_{pore} \quad (5)$$

where ε_{ii} is the volumetric strain tensor; and p_{pore} is the pore pressure, which can be replaced by the average pore pressure $\overline{p}$. If the porosity change induced by water pressure must be studied, Q should be considered in both Equations (5) and (3).

According to previous research on the average pore pressure (Lewis and Schrefler 1982), because the air pressure is assumed to be zero in this paper, $\overline{p}$ can be defined as:

$$\overline{p} = S_w p^w \quad (6)$$

According to Equations (5) and (6), with the assumption of $\zeta = 1$, the dynamic porosity can be expressed as:

$$\upsilon = \frac{\upsilon_0 + \varepsilon_{ii} + \frac{1}{K_s}(S_w p^w - S_{w0} p_0)}{1 + \frac{1}{K_s}(S_w p^w - S_{w0} p_0)} \quad (7)$$

where υ_0 is the initial porosity, p_0 is the initial water pressure, and S_{w0} is the initial water saturation.

Equation (7) with Equations (4) and (2) build the general mathematical model for hydro-mechanical coupling in unsaturated soil with dynamic porosity (UHM-P). This model considers porosity change due to deformation (mechanical behavior) and pore pressure (hydraulic behavior). The UHM-P model degrades to the UHM model if the porosity change is ignored.

Deformation energy equation

The deformation energy W (i.e., the dual potential) describes the potential that controls the deformation (Chen and Hicks 2011). Its time derivative $\dot{W}$ in soil with consideration of dynamic porosity change υ is defined as:

$$W = \left(\Psi - \upsilon\psi_{pore}\right) - \overline{p}\upsilon \tag{8}$$

$$\dot{W} = tr(\mathbf{T}\dot{\mathbf{E}}) - \dot{\overline{p}}\,\upsilon \tag{9}$$

where $\Psi = J\psi$ is the Helmholtz free energy density in the reference configuration of the total soil, J is the Jacobian deformation gradient $\mathbf{F}$, ψ_{pore} is the Helmholtz free energy density of the pore water, $\mathbf{T}$ is the second Piola-Kirchhoff stress, and $\mathbf{E}$ is the Green strain.

Critically, the dynamic evolution of porosity influences deformation energy, which has remained unclear in previous research. Substituting Equation (6) into (8) and (9) leads to:

$$W = \left(\Psi - \upsilon\psi_{pore}\right) - S_w p\upsilon \tag{10}$$

$$\dot{W} = tr(\mathbf{T}\dot{\mathbf{E}}) - (S_w p)^{\boldsymbol{\cdot}}\,\upsilon \tag{11}$$

The deformation energy is the energy obtained by deducting the energy of pore water pressure from the energy of the soil matrix, and its time derivative is a function of $\mathbf{E}$, p and υ. With the small strain assumption, the Green Strain tensor E_{ij} and Piola-Kirchhoff stress T_{ij} can be replaced by the strain tensor ε_{ij} and Cauchy stress σ_{ij}. Therefore, equation (11) becomes:

$$\dot{W} = tr(\begin{bmatrix} \varepsilon_{11} & \varepsilon_{12} & \varepsilon_{13} \\ \varepsilon_{21} & \varepsilon_{22} & \varepsilon_{23} \\ \varepsilon_{31} & \varepsilon_{32} & \varepsilon_{33} \end{bmatrix} \begin{bmatrix} \dot{\sigma}_{11} & \dot{\sigma}_{12} & \dot{\sigma}_{13} \\ \dot{\sigma}_{21} & \dot{\sigma}_{22} & \dot{\sigma}_{23} \\ \dot{\sigma}_{31} & \dot{\sigma}_{32} & \dot{\sigma}_{33} \end{bmatrix}) - (S_w p)^{\boldsymbol{\cdot}} \upsilon \tag{12}$$

Methodology

Numerical model

The UHM model and UHM-P model are validated and analyzed in this study by considering the simple but classic coupled hydraulic-mechanical problem of unsaturated "triaxial test" experiments. The experimental data come from two published articles (Vassallo et al. 2007), and (Biglari et al. 2012). In these experiments, soil samples were kept unsaturated throughout the entire period. After obtaining some basic soil parameters, such as the plastic limit and initial water content, a sample of height H and width W was mounted in the test apparatus (Fig. 1). The controlling water pressure on the lower boundary (P_w) and the air pressure on the upper boundary (P_a) are maintained to ensure that the suction $S = P_a - P_w$ remains constant. Concurrently, the mean net stress $|\sigma| = P - P_a$ on the upper and lateral boundaries is also a constant. This procedure is called the equalization stage, when the sample swells or compresses according to its initial water content. The equalization stage ends when the pore water content and total soil volume stabilize. Then, isotropic compression is performed, and this stage gradually increases the mean net stress to a final value. A loading rate of 4 kPa/h is used by Vassallo to ensure fully drained and constant suction conditions. The pore water content and volume change of the sample were measured during these experiments. The 2D numerical model is shown in Fig. 1.

To solve the model equations, COMSOL Multiphysics software was used to build a numerical model. Darcy's law was used for the hydraulic field, and the linear elastic materials model was used for the mechanics field. The initial displacement of the sample (d_0) was zero. The initial water pressure (P_0) was calculated from the initial water content using the Van Genuchten equation (Genuchten and Th. 1980). The upper and right pressure boundaries for the mechanics field were pressure boundaries, and the stress σ was $P\text{-}P_a$. The lower boundary was a 'roller' boundary, indicating no vertical deformation. The upper and right boundaries for the hydraulic field were no flow boundaries; the lower boundary was a fixed pressure boundary with a pressure value equal to -S; and the left boundary was a symmetric boundary. All simulation settings and sample parameters used for model validation are shown in Table 1. The Young's modulus, Poisson's ratio and poroelastic storage are reported in Alonso's studies (Alonso and Alcoverro 1999a, Alonso and Alcoverro 1999b). The Van Genuchten equation parameters were obtained by fitting the experimental water content and water pressure. The porosity used in the UHM model is a constant value, which is the initial porosity value in the UHM-P model, as the porosity changes during evolution.

Model validation method

The modeled change of specific water volume in the equalization stage by Vassallo and Biglari was compared with the experimental change. The specific water volume v_w was calculated using the model result:

$$v_w = G_s w = G_s S_w \upsilon \tag{13}$$

where G_s is the specific gravity of the soil solids and w is the water content.

Note that the sample was divided into many elements in the model; thus, the surface average saturation was used to calculate the v_w of the total sample.

For validation using results of both Vassallo and Biglari, the experimental data from one sample were used for the model's calibration; however, experimental data from all samples were used for validation.

The error between the model results and experimental data was quantified using the following equations during calibration and validation:

$$AVRE = \sum_{i=1}^{n} \left| M_i / E_i \right| / n \tag{14}$$

$$R = \frac{\sum_{i=1}^{n} \left(M_i - \overline{M} \right)\left(E_i - \overline{E} \right)}{\sqrt{\sum_{i=1}^{n} \left(M_i - \overline{M} \right)^2 \bullet \sum_{i=1}^{n} \left(E_i - \overline{E} \right)^2}} \tag{15}$$

where $AVRE$ is the relative average error and R is the correlation coefficient. In Equations (14) and (15), M_i is the model value, E_i is the experimental value, n is the total number of data points, $\overline{M}$ is the average of the model data, and $\overline{E}$ is the average of the experimental values.

Sensitivity analysis method

To describe the effect of parameter variation on the change in model calculation more accurately, the ratio of parameter variation (ROV) (Cheviron and Coquet 2009) was used. This variation relates the relative variation in the results to analyze the parameter sensitivity. Four primary parameters were chosen: permeability (k), poroelastic storage (q), Biot's coefficient (ζ) and Young's modulus (E). The average specific water content, average volumetric strain for the hydraulic results and mechanical results were chosen separately. The ROV was calculated using:

$$ROV(t) = \frac{\left[c(t) - c_{ref}(t) \right] / \left| c_{ref}(t) \right|}{\left(p - p_{ref} \right) / p_{ref}} = \frac{out\,\mathrm{var}}{in\,\mathrm{var}} \tag{16}$$

The reference model is the model of sample 'E' that is validated by the experimental data of Biglari's results. $c_{ref}(t)$ is the calculated value of the reference model at a specified time, p_{ref} is the parameter value of the reference model, $c(t)$ is the calculated value of the variation model with the parameter changed and p is the parameter value of the variation model.

During each calculation of the sensitivity analysis, one parameter was changed, and the other parameters were held constant. Then, the sensitivity to that parameter was analyzed using ROV. The calculated value changes with time; thus, a maximum, average and minimum value are defined for each parameter as:

$$\begin{aligned} ROV_{\max} &= \max\left|ROV(t)\right| \\ ROV_{\min} &= \min\left|ROV(t)\right| \\ ROV_{ave} &= \sum_{t=0}^{t=T} ROV(t)/N \end{aligned} \tag{17}$$

where $ROV_{\max}$ is the maximum effect of parameter change to the calculation value in the total period and is the maximum absolute value of ROV of one parameter during the calculation period; $ROV_{\min}$ is the minimum effect of parameter change and the ROV of minimum absolute value; ROV_{ave} is the average sensitivity of parameter and is the average value of ROV in the calculation period; N is the number of ROV; and T is the end time.

All of the input variations for parameters in the sensitivity analysis are shown in Table 2. These parameters varied from -60% to 60% compared to their reference value. The variation ranges of ζ and E are based on previous studies by (Alonso and Alcoverro 1999b) and (Selvadurai et al. 2019).

Model validation results

In this section, the results of the UHM model are compared with the experimental data, and the result error of each sample is analyzed. Comparisons of the experimental and modeled changes in specific water volume Δv_w of four samples in researches of Vassallo and Biglari are shown in Fig. 2 and Fig. 3, respectively.

The experimental data in Fig. 3 are smoother than those in Fig. 2 due to the finer measurement techniques used by Biglari. Different responses of Δv_w can be observed in the eight samples. The water content rises in all samples except for S100P400TG, samples F and G, which implies that the initial water pressures of S100P400TG, samples F and G, were higher than the water pressure on the lower boundary (i.e., these samples drain during the equalization period). For the other samples, the water pressure on the lower boundary is higher than the initial water pressure; thus, the water flows to the upper part of the sample from the lower boundary (i.e., there is a rising saturation in these wetting samples, and Δv_w remains positive).

The rise of Δv_w slows and reaches zero after approximately 12,000 minutes for the samples in Vassallo's study. The initial Δv_w error of S100P100TG is higher than that of the other three samples, which may be due to inexact measurement of the initial water pressure in that sample.

The calculated error for each sample of Vassallo's study is shown in Table 3. The $AVRE$ of all samples are low except for S100P100TG. R is larger than 0.9 in all samples, showing a good correspondence between the experimental data and model results.

The rise in Δv_w also slows for samples in Biglari's study. Equalization is reached in approximately 40 h. The permeability of samples in Biglari's study is larger than that in Vassallo's, and the water pressure changes in Biglari's are also larger. These two factors promote faster pore water flow through samples in Biglari's study, thus shortening equalization time. The model results are less accurate at D, showing marked positive errors at both early and late stages, compared with the other samples. The calculated error for each sample is shown in Table 4. The $AVRE$ and R of all samples are generally better than those in Vassallo's study and acceptable in numerical calculation.

Nearly all sample errors are positive throughout the calculation period. However, the errors between the experimental data and model results differ between samples that drain and wet. Most errors in the modeling results of draining samples are higher in the early stage and lower in the late stage, while wetting samples exhibit an opposite trend.

Sensitivity analysis of model parameters

The sensitivity of permeability k, poroelastic storage q, Biot's coefficient ζ and Young's modulus E of the UHM model were assessed using the ratio of parameter variation (ROV). The parameter value of the reference model comes from a previous study of clay and silt soil. Therefore, we investigated a relatively tight range of -60% to 60%, where ζ is -60% to -30%, to make specific statements about the sensitivity of parameters of soft soil instead of covering general variation of parameters for all soils. The variation range for all parameters is the same; thus, we can compare the sensitivity of each parameter without the influence of parameter value because all the sensitivity of parameters is parameter value-dependent.

Parameter sensitivity of mechanical behavior

The average volumetric strain of the sample using different input parameter values is shown in Fig. 4. In all cases, the volumetric strain increases rapidly in the early stage, reaches its peak, and then decreases slowly back to its initial value. The opposite effect of permeability and poroelastic storage on the volumetric strain is clearly shown. The peak volumetric strain is delayed with decreasing k, and the curves also become smoother. However, the decrease in q hastens the appearance of the peak volumetric strain and the final equilibrium value, making the curves steeper. Also, the peak value of the volumetric strain increases with increasing q, while the variation in k shows nearly no effect on the peak value of the volumetric strain.

The variation in ζ seems to have little effect on the volumetric strain. The change in the volumetric strain using a variation of ζ to the reference value is small, and the maximum difference is only approximately 2×10^{-7}. The shape of the curve does not change with the variation of ζ. However, the variation in Young's modulus E (the parameter of direct determination of the stress–strain relationship) exhibits a strong effect. Variation in E leads to different initial and end values of the volumetric strain, and the peak value changes from approximately -1.7×10^{-4} to -6.7×10^{-3}. A change in E also has no effects on the time to equilibrium of volumetric strain, with all curves of different E becoming horizontal lines after approximately 30 h.

The ROV for each parameter for average volumetric strain is shown in Table 5.

Table 5 shows that the average ROV of different parameters varies considerably within a range of -0.0034 to 2.5015. The higher $|ROV|$ is, the more sensitive parameter is. A positive value means that the calculation results are positively correlated with parameters, while a negative value means a negative correlation.

The model appears to be more sensitive to E than all other parameters with respect to ROV_{ave}, ROV_{max} and ROV_{min}. There is little change between ROV_{max} and ROV_{min} for E at one specific value, which shows that the sensitivity of E is stable throughout the calculation period. Therefore, the strain or displacement evolution does not affect the sensitivity of E, as observed in another study (Abdollahipour et al. 2019). The peak value of the ROV for E appears at the initial time. The ROV for ζ are small and steady, and have negative effects on the results.

The ROV value for k and q change markedly throughout the calculation period. The ROV of k is positive in the early stage (i.e., before the peak of volumetric strain) and changes to a negative value after the peak. The ROV of q actually exhibits the opposite trend. As the parameter increases, ROV_{ave} of E and k significantly decreases, indicating that these two parameters are more sensitive at low values.

Similarly, other research (Jin et al. 2016) has shown that displacement is more sensitive to these two parameters of low value in a saturated 3D model using Biot's equation. The ROV_{ave} of q and ζ remain nearly stable during the variation, exhibiting strong symmetry.

Parameter sensitivity of hydraulic behavior

The variation in specific water content Δv_w of the sample using different input parameter values is shown in Fig. 5. Δv_w begins at 0 and rises to the same value, with the rates of Δv_w change decreasing with time. The model suggests that k and q also have opposite influences on the specific water content. As k increases, the rate of increase of Δv_w increases and reaches its final value earlier. However, as q increases, the rate of increase of Δv_w decreases, and the time to reach its final value lengthens. The ROV of k and q change throughout the calculation period. The ROV of k is always positive but decreases to nearly 0 at the end. The ROV_{min} of -60% variation of k is 0.0140 because in this case, it does not reach a steady state at the end of the simulation. Conversely, the ROV of q remains negative in the model, which is to be expected, as the increase in k promotes the water flow and shorten the time to water pressure equalization according to Equation (4), while q has a negative effect on the water pressure change.

As with volumetric strain, ζ has a weak influence on Δv_w, with little effect on the basic shape of the curve. The influence of the change in E on Δv_w is also small; however, the pattern of change is unusual. Close inspection of the curve between 30 h and 44 h shows that the value of E= 2.428×10^8 is initially lower than that of E= 1.670×10^8 but surpasses the latter after a few hours and then decreases again 5 h later. In general, low values for E contribute to the highest value of Δv_w.

The ROV of each parameter for the specific water content is shown in Table 6.

Analysis of the advantages and limitations of the new Model

The validation described in the previous chapter is based on the UHM model. In this chapter, the new model (UHM-P) is compared with the results of the UHM model, and the limitation of the new model is analyzed in detail.

Influence of porosity change on hydraulic and mechanical behavior

As discussed before, during the equalization stage, the variation of the model from the experimental results for draining and wetting samples appears to display different trends. Fig. 6a shows the variation in calculation error of Δv_w for samples E and G using the UHM model. This figure clearly shows that the error for sample E increases to approximately 0.002 in the first few hours and then decreases to 0.0001 at and beyond 20 h. However, for sample G, the error decreases to approximately -0.002 within 6 hours and then increases and remains at 0.002 after 20 h. These trends can be explained by the porosity change during the model period. A value of 5×10^{10} Pa for K_s (Alonso and Alcoverro 1999a) was selected to calculate the theoretical true porosity. Fig. 6b shows the theoretical true porosity during the equation stage. The porosities of both E and G are lower than the initial porosity of 0.539 due to the confining pressure, while the UHM model assumes a constant value for porosity. This result may overstate the true porosity during the experimental period, contributing to the positive errors in most of the models (see Equation (13)). The evolution of porosity in E and G are different. As discussed earlier, the water pressures in sample E increase during the experiments, while those in G decrease. Therefore, the water pressure changes induced different changes in porosity. Water pressure shows a positive effect during the late stage of E (the final porosity is higher than the earlier porosity), while the opposite impact was found during the late stage of G.

The constant porosity value is replaced with the theoretical dynamic porosity obtained by Equation (7) in the UHM-P model. The results of the equalization stage by the UHM-P model are shown in Fig. 7. For both samples, the modified results are lower than the original model results. Modification of the model reduces the error caused by the overvaluation of porosity during the experiment. As mentioned above, the porosity change is relatively small in the equalization stage; however, the porosity change still strongly influences the numerical calculation. Table 7 shows that the AVRE of the results improves markedly for both samples E and G. The average relative error of E decreases from approx. 0.0985 to 0.0543 (a 44.9% improvement in relative error), while this error of G decreases from approx. 0.0962 to 0.0623 (a 35.2% improvement in relative error). However, the modification seems to have no marked effect on R.

Fig. 8 shows the modeled results of $\log(p - p_a) : V$ during the isotropic compression stage of Vassallo's study, where V is the specific volume, which is calculated by:

$$V = 1 + e = 1 + \frac{\upsilon}{1\text{-}\upsilon} \tag{1}$$

The modeled result of V remains zero if the porosity change is not considered in the model. The maximum porosity change reached 0.040 (9.2% less than the initial porosity) in S100CI and 0.036 (8.3% less than the initial porosity) in S200CI. The porosity change during the isotropic compression stage is much larger than that during the equalization stage. Therefore, porosity change is also important when studying the mechanical behavior of soil.

Model limitations

The proposed model is based on mixture coupling theory, which has the advantage of engaging multiscale coupled processes, by analyzing the Helmholtz free energy difference between the pore water and the wetted matrix.

Compared with the previous model, the proposed model considers the evolution of porosity and yields the dynamic porosity equation in the hydro-mechanical model. Several assumptions were made to simplify the discussion, including the following: the soil is homogeneous, isotropic, and linearly elastic during deformation; the coupling coefficient ζ, Q and the elastic stiffness are all material-dependent, which means that they remain constant in a specific material. Therefore, the model cannot manage large- or plastic-deformation problems. Additionally, because some soils may experience modulus changes under different suctions (Sawangsuriya et al. 2009), the proposed model must be modified when dealing with such problems.

Another limitation is that all of the pore space is assumed to be isotropic in the hydraulic flow, which may lead to large errors with fractured media. In this model, air is assumed to always remain at a fixed pressure, p_{atm}, and the air is continuous. These assumptions ensure that no air flows in the porous media. Although the air influence on liquid flow can be considered, the model cannot be used to solve a two-phase flow problem in deformed porous media.

For some rocks, permeability change is more sensitive than porosity change (Raghavan and Chin 2004), and the proposed model, which ignores permeability change, may face difficulty in such a problem. Finally, this study focuses on experimental validation and porosity changes on a relatively small scale. Water density variations in space and time are not considered in the model, which may be important in field studies or in research focusing on intensive pressure changes.

Influence of porosity change on deformation energy

Fig. 9 shows the evolution of deformation energy at the center of samples E and G with and without considering porosity change. This figure shows the influence of porosity change on deformation energy. The time derivative of deformation energy $W^{\cdot}$ is positive in sample E but remains negative in sample G. The $W^{\cdot}$ of sample E decreased to approximately -0.2335 in the early stage and then increased to approximately 0 at the end. While the $W^{\cdot}$ of G exhibited the opposite trend compared with E, the peak of $W^{\cdot}$ appears at approximately 1.95 h in E and at approximately 0.58 h in G and is consistent with the peak of water pressure, which is confirmed in Equation (12).

Similarly, the calculation error of $W^{\cdot}$ is different in the two samples caused by the porosity change. The $W^{\cdot}$ that considers porosity change is always higher than that that does not in sample E, while the $W^{\cdot}$ that considers porosity change is always lower than that does not in sample G. These results are due to the different evolution of water pressure in samples E and G. Water pressure of sample E increased during experiment, while the water pressure of sample G decreased, resulting in positive and negative time derivative of water pressure in samples E and G, respectively. The calculation error index AVRE of $W^{\cdot}$ that does not consider porosity change in sample E is approximately 1.00051; in sample G, the AVRE is approximately 1.00053.

The 2D contour maps of $W^{\cdot}$ of samples E and G are shown in Fig. 10 and Fig. 11. These two figures show interesting evolutions of $W^{\cdot}$ at different subzones of the total sample. The $W^{\cdot}$ of the lower part is markedly higher than that of the upper part in the beginning. Then, the high value subzone moves up over time, and finally, the $W^{\cdot}$ of the upper part is higher than that of the lower part. This trend indicates that the lower part of the sample deforms much earlier than the upper part in the experiment. In addition, the absolute value of $W^{\bullet}$ in the early stage is higher than that in the later stage, which means that the deformation is stronger in the early stage than in the later.

This evolution is similar in sample G. A higher absolute value of $W^{\bullet}$ is shown in the lower part at the beginning, and a higher absolute value of the upper part is shown in the end. Additionally, a marked decrease is observed in the absolute value of $W^{\bullet}$ in the total sample over time.

In this numerical analysis, no additional volume force was loaded on the sample except for the small confined pressure in the lateral direction. The deformation is primarily due to the water pressure change, which is caused by water absorption in sample E and water drainage in sample G. The calculation results of the first term in Equation (11) , $tr(\mathbf{T}\dot{\mathbf{E}})$ (range about 4×10^{-5} to 3×10^{-4}), is much lower than the second term $(S_w p)^{\bullet}\upsilon$, which explains the negative value of $W^{\bullet}$ in sample E and the positive value in sample G.

The deformation energy is useful in the analysis of the coupling behavior of soil. The lower boundary is the constant water pressure in this analysis. The water pressure change begins at the lower part of the samples, and the change in W and deformation also begins at the lower part. The decrease in the absolute value of $W^{\bullet}$ is caused by the decrease in the water pressure change rate in the samples. When the water pressure reached an equilibrium value, $W^{\bullet}$ reached nearly zero, and then the deformation energy W finally stabilized, leading to a new steady stage of the samples (i.e., no further deformation).

Conclusion

In this study, a new coupled unsaturated hydromechanical model considering dynamic porosity ((UHM-P) for soil was developed. The experimental data for two different unsaturated triaxial tests were used to validate this model. Validation shows that the UHM-P model can basically describe the hydro-mechanical multifield behavior in unsaturated soil, when ignoring porosity changes. The average relative errors of all the experimental samples are between 0.8631 and 1.3046, and all the correlation coefficients are between 0.9028 and 0.9981.

Sensitivity analysis shows that Young's modulus (E) is the most sensitive parameter in the calculation of volumetric strain, followed by permeability (k). The sensitivity of the model to poroelastic storage (q) and Biot's coefficient (ζ) seems to be stable over a range of parameter values, while the sensitivities of k and E are higher at low values. The modeled hydraulic behavior is most sensitive to k , followed by q . The sensitivity of ζ is also stable over a range of parameter values, while the sensitivity of the other three parameters is higher at low values.

Modeled results show that the UHM model cannot calculate the specific volume change. Even during the relatively low deformation stage, the calculation results of the specific water volume are more realistic when the dynamic porosity is considered, leading to 44.9% and 35.2% improvements in the relative error in samples E and G, respectively.

The deformation energy results show that the relative calculation error when not considering porosity change is approximately 0.00051 and 0.00053 in samples E and G, respectively.

Data Availability Statement

Some or all data, models, or code that support the findings of this study are available from the corresponding author upon reasonable request (Numerical model).

Acknowledgment

This study was supported by the National Key R&D Program of China (No. 2019YFC1805503), the National Key R&D Program of China (No. 2018YFC1800905) and the Key Science and Technology Projects of the Inner Mongolia Autonomous Region (2019ZD001).

References

Abdollahipour, A., H. Soltanian, Y. Pourmazaheri, E. Kazemzadeh and M. Fatehi-marji. 2019. "Sensitivity analysis of geomechanical parameters affecting a wellbore stability " *J. Cent. South Univ.* 26 (03): 768-778.

Alonso, E. E. and J. Alcoverro 1999a. Catsius Clay Project. Calculation and Testing of Behaviour of Unsaturated Clay as Barrier in Radioactive Waste Repositories. Stage 2: Validation Exercises at Laboratory scale. Spain.

Alonso, E. E. and J. Alcoverro 1999b. Catsius Clay Project: Calculation and testing of behaviour of unsaturated clay as barrier in radioactive waste repositories: stage 3: validation exercises at a large in situ scale, Empresa Nacional de Residuos Radiactivos.

Biglari, M., A. d'Onofrio, C. Mancuso, M. K. Jafari, A. Shafiee and I. Ashayeri. 2012. "Small-strain stiffness of Zenoz kaolin in unsaturated conditions." *Can. Geotech. J.* 49 (3): 311-322. https://doi.org/10.1139/t11-105.

Biot, M. A. 1941. "General theory of three-dimensional consolidation." *J. Appl. Phys.* 12 (2): 155-164. https://doi.org/10.1063/1.1712886.

Biot, M. A. 1962. "Mechanics of Deformation and Acoustic Propagation in Porous Media." *J. Appl. Phys.* 33 (4): 1482-1498. https://doi.org/10.1063/1.1728759.

Charlier, R., F. Collin, B. Pardoen, J. Talandier, J.-P. Radu and P. Gerard. 2013. "An unsaturated hydro-mechanical modelling of two in-situ experiments in Callovo-Oxfordian argillite." *Eng. Geol.* 165: 46-63. https://doi.org/10.1016/j.enggeo.2013.05.021.

Chen, X. and M. A. Hicks. 2011. "A constitutive model based on modified mixture theory for unsaturated rocks." *Comput. Geotech.* 38 (8): 925-933. https://doi.org/10.1016/j.compgeo.2011.04.008.

Chen, X. and M. A. Hicks. 2013a. "Unsaturated hydro-mechanical-chemo coupled constitutive model with consideration of osmotic flow." *Comput. Geotech.* 54: 94-103. https://doi.org/10.1016/j.compgeo.2013.06.001.

Chen, X., W. Pao and X. Li. 2013b. "Coupled thermo-hydro-mechanical model with consideration of thermal-osmosis based on modified mixture theory." *Int. J. Eng. Sci.* 64: 1-13. https://doi.org/10.1016/j.ijengsci.2012.12.005.

Chen, X., W. Pao, S. Thornton and J. Small. 2016. "Unsaturated hydro-mechanical-chemical constitutive coupled model based on mixture coupling theory: Hydration swelling and chemical osmosis." *Int. J. Eng. Sci.* 104: 97-109. https://doi.org/10.1016/j.ijengsci.2016.04.010.

Chen, X., S. F. Thornton and W. Pao. 2018. "Mathematical model of coupled dual chemical osmosis based on mixture-coupling theory." *Int. J. Eng. Sci.* 129: 145-155.

https://doi.org/10.1016/j.ijengsci.2018.04.010.

Chen, Y.-F., J.-M. Hong, H.-K. Zheng, Y. Li, R. Hu and C.-B. Zhou. 2016. "Evaluation of Groundwater Leakage into a Drainage Tunnel in Jinping-I Arch Dam Foundation in Southwestern China: A Case Study." *Rock Mech. Rock Eng.* 49 (3): 961-979. https://doi.org/10.1007/s00603-015-0786-y.

Cheviron, B. and Y. Coquet. 2009. "Sensitivity Analysis of Transient-MIM HYDRUS-1D: Case Study Related to Pesticide Fate in Soils." *Vadose Zone J.* 8 (4): 1064-1079. https://doi.org/10.2136/vzj2009.0023.

Edip, K., V. Sesov, C. Butenweg and J. Bojadjieva. 2018. "Development of coupled numerical model for simulation of multiphase soil." *Comput. Geotech.* 96: 118-131. https://doi.org/10.1016/j.compgeo.2017.08.016.

Félix, B., P. Lebon, R. Miguez and F. Plas. 1996. "A review of the ANDRA's research programmes on the thermo-hydromechanical behavior of clay in connection with the radioactive waste disposal project in deep geological formations." *Eng. Geol.* 41 (1): 35-50. https://doi.org/10.1016/0013-7952(95)00025-9.

Genuchten, V. and M. Th. 1980. "A closed-form equation for predicting the hydraulic conductivity of unsaturated soils." *Soil Science Society of America Journal* 44 (5): 892-898. 10.2136/sssaj1980.03615995004400050002x.

Heidug, W. K. and S. W. Wong. 1996. "HYDRATION SWELLING OF WATER-ABSORBING ROCKS: A CONSTITUTIVE MODEL." *Int. J. Numer. Anal. Methods Geomech.* 20 (6): 403-430. https://doi.org/10.1002/(SICI)1096-9853(199606)20:6<403::AID-NAG832>3.0.CO2-7.

Jin, W.-z., Z.-j. Luo and X.-h. Wu. 2016. "Sensitivity analysis of related parameters in simulation of land subsidence and ground fissures caused by groundwater exploitation." *Bull. Eng. Geol. Environ.* 75 (3): 1143-1156. https://doi.org/10.1007/s10064-016-0897-z.

Lewis, E. R., K. Morgan, B. Schrejler, E. Hinton, P. Bettess, O. Zienkiewicz, E. C. Desai, R. Gallagher, R. Wood and J. Alex. 1987. "The finite element method in the deformation and consolidation of porous media."

Lewis, R. and B. Schrefler 1982. *Finite element simulation of the subsidence of a gas reservoir undergoing a waterdrive*. *Finite element in fluids*, John Wiley & Sons,Ltd. **4:** 179-199.

Li, W. and Q. Yang. 2018. "Hydromechanical Constitutive Model for Unsaturated Soils with Different Overconsolidation Ratios." *Int. J. Geomech.* 18 (2): 04017142. doi:10.1061/(ASCE)GM.1943-5622.0001046.

Li, X., R. Li and B. A. Schrefler. 2006. "A coupled chemo-thermo-hygro-mechanical model of concrete at high temperature and failure analysis." *Int. J. Numer. Anal. Methods Geomech.* 30 (7): 635-681. https://doi.org/10.1002/nag.495.

Lisjak, A., P. Kaifosh, L. He, B. S. A. Tatone, O. K. Mahabadi and G. Grasselli. 2017. "A 2D, fully-coupled, hydro-mechanical, FDEM formulation for modelling fracturing processes in discontinuous, porous rock masses." *Comput. Geotech.* 81: 1-18. https://doi.org/10.1016/j.compgeo.2016.07.009.

Ma, Y., X. H. Chen, L. J. Hosking, H. S. Yu, H. R. Thomas and S. Norris. 2021. "The influence of coupled physical swelling and chemical reactions on deformable geomaterials." *Int. J. Numer. Anal. Methods Geomech.* 45 (1): 64-82. https://doi.org/10.1002/nag.3134.

Masoudian, M. S., M. A. Hashemi Afrapoli, A. Tasalloti and A. M. Marshall. 2019. "A general framework for coupled hydro-mechanical modelling of rainfall-induced instability in unsaturated slopes with multivariate random fields." *Comput. Geotech.* 115: 103162. https://doi.org/10.1016/j.compgeo.2019.103162.

Meroi, E. A., B. A. Schrefler and O. C. Zienkiewicz. 1995. "LARGE-STRAIN STATIC AND DYNAMIC SEMISATURATED SOIL BEHAVIOR." *Int. J. Numer. Anal. Methods Geomech.* 19 (2): 81-106. https://doi.org/10.1002/nag.1610190203.

Raghavan, R. and L. Y. Chin. 2004. "Productivity changes in reservoirs with stress-dependent permeability." *Spe Reservoir Evaluation & Engineering* 7 (4): 308-315. 10.2118/88870-pa.

Sanavia, L., B. A. Schrefler and P. Steinmann. 2002. "A formulation for an unsaturated porous medium undergoing large inelastic strains." *Comput. Mech.* 28 (2): 137-151. https://doi.org/10.1007/s00466-001-0277-8.

Sawangsuriya, A., T. B. Edil and C. H. Benson. 2009. "Effect of Suction on Resilient Modulus of Compacted Fine-Grained Subgrade Soils." *Transp. Res. Record* (2101): 82-87. 10.3141/2101-10.

Schwartz, M. O. 2018. "Modelling groundwater contamination above a potential nuclear waste repository in the Columbia River Basalt, USA." *Environ. Earth Sci.* 77 (12): 1-12. https://doi.org/10.1007/s12665-018-7615-z.

Seetharam, S. C., H. R. Thomas and P. J. Cleall. 2007. "Coupled thermo/hydro/chemical/mechanical model for unsaturated soils - Numerical algorithm." *Int. J. Numer. Meth. Eng.* 70 (12): 1480-1511. https://doi.org/10.1002/nme.1934.

Selvadurai, P., P. A. Selvadurai and M. Nejati. 2019. "A multi-phasic approach for estimating the Biot coefficient for Grimsel granite." *Solid Earth* 10 (6): 2001-2014. https://doi.org/10.5194/se-10-2001-2019.

Stormont, J. C. and J. J. K. Daemen. 1992. "Laboratory Study of Gas Permeability Changes in Rock Salt During Deformation." *Int. J. Rock Mech. Min.* 29 (4): 325-342. 10.1016/0148-9062(92)90510-7.

Terzaghi, K. 1943. *Theory of Consolidation*. *Theoretical Soil Mechanics*: 265-296.

Truesdell, C. 1962. "Mechanical Basis of Diffusion." *J. Chem. Phys.* 37 (10): 2336-2344. https://doi.org/10.1063/1.1733007.

Vassallo, R., C. Mancuso and F. Vinale. 2007. "Effects of net stress and suction history on the small strain stiffness of a compacted clayey silt." *Can. Geotech. J.* 44 (4): 447-462. https://doi.org/10.1139/t06-129.

Zhang, R., Z. Liu, J. Zheng and J. Zhang. 2020. "Experimental Evaluation of Lateral Swelling Pressure of Expansive Soil Fill behind a Retaining Wall." *J. Mater. Civ. Eng.* 32 (2). https://doi.org/10.1061/(asce)mt.1943-5533.0003032.

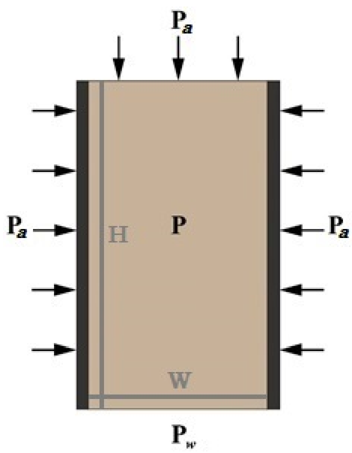

Fig. 1. 2D Numerical model domain and conditions

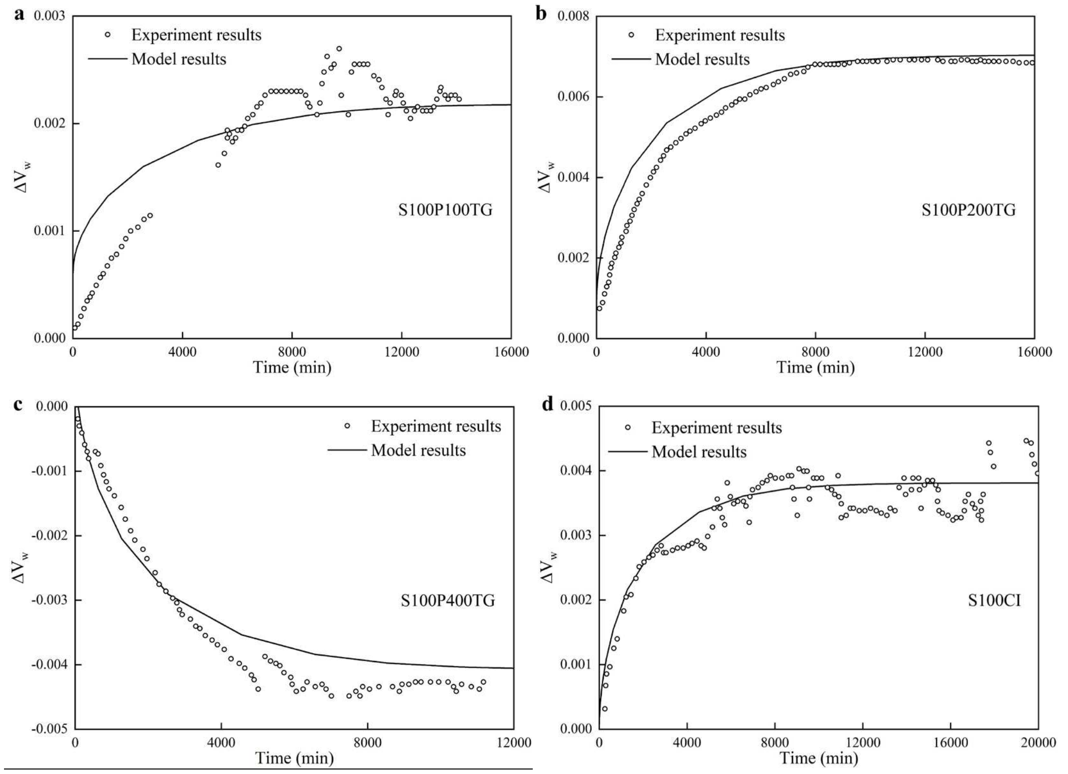

Fig. 2. Comparison of experimental and model results for Δv_w in Vassallo's test, a for sample S100P100TG, b for sample S100P200TG, c for sample S100P400TG and d for sample S100CI

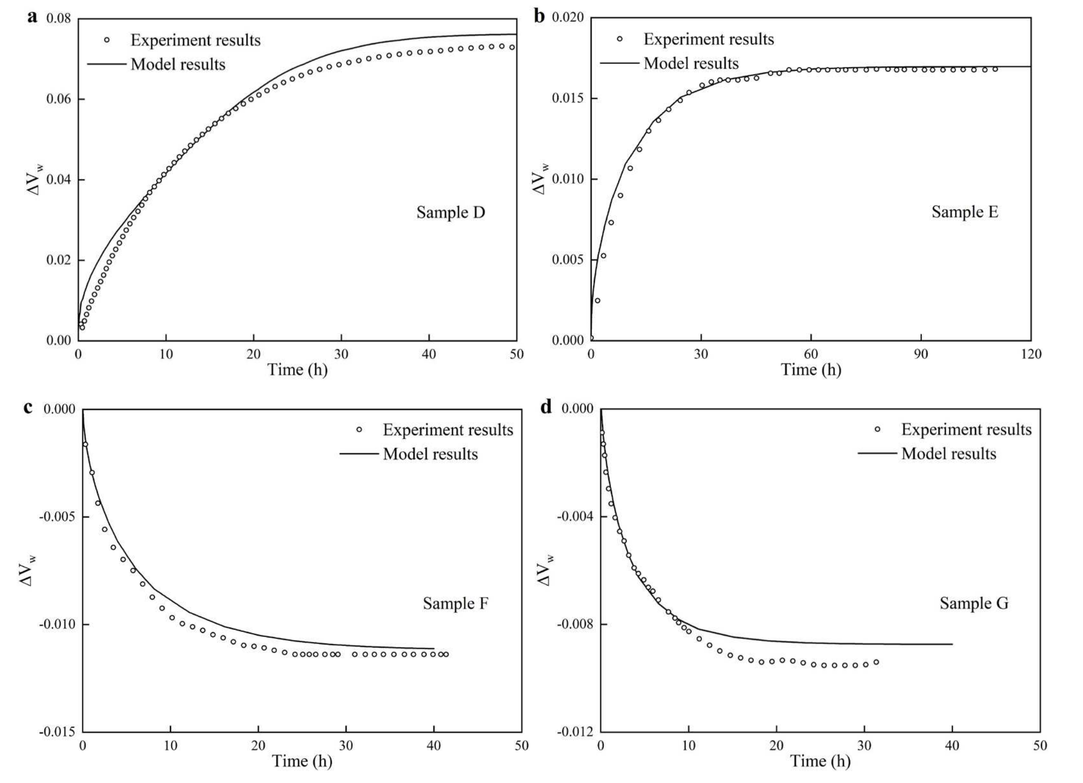

Fig. 3. Comparison of experimental and model results for Δv_w in Biglari's test, a for Sample D, b

for Sample E, c for Sample F and d for Sample G

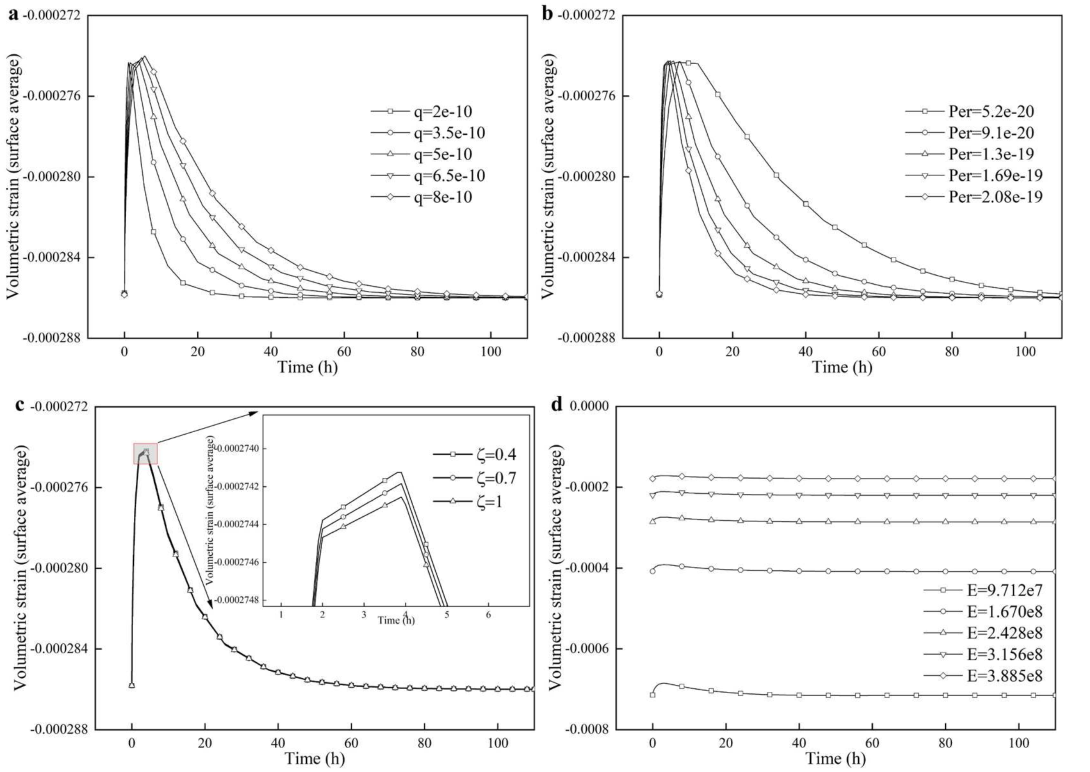

Fig. 4. Different responses of average volumetric strain to the variation of input parameters, a for poroelastic storage, b for permeability, c for Biot's consolidation coefficient and d for Young's modulus

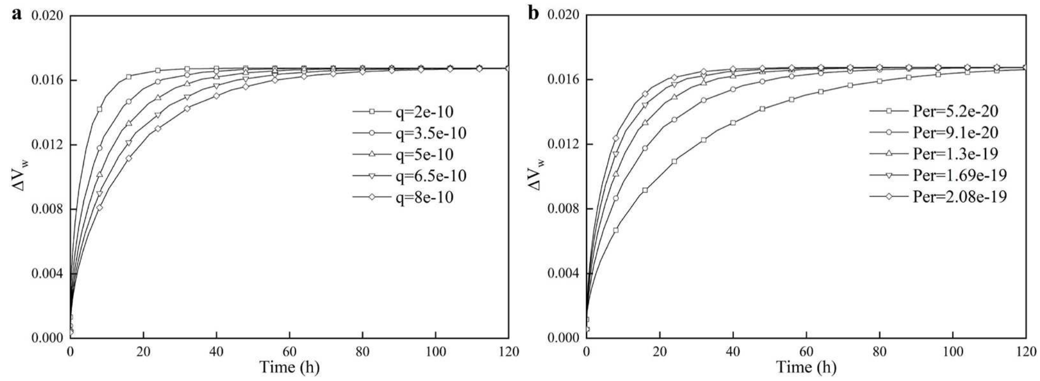

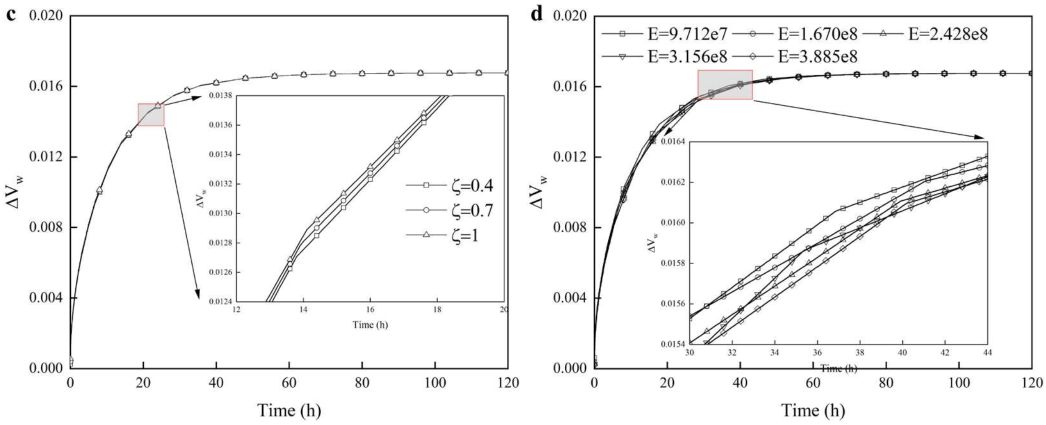

Fig. 5. Different responses of Δv_w to the variation in input parameters, a for poroelastic storage, b for permeability, c for Biot's consolidation coefficient and d for Young's modulus

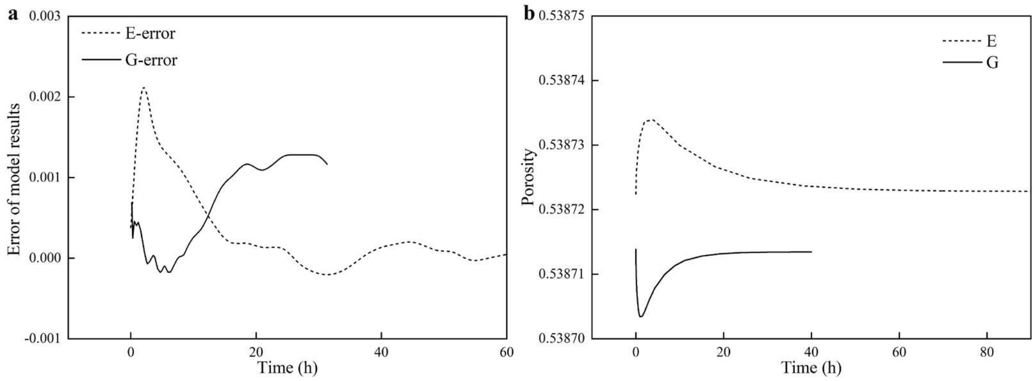

Fig. 6. a for the calculation error of the UHM model and b for the theoretical porosity calculated by the UHM-P model during experimentation

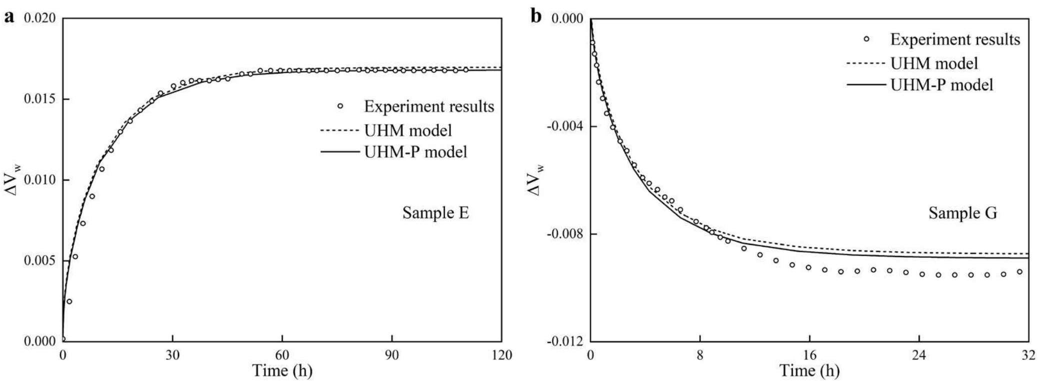

Fig. 7. Experimental Δv_w and model results with (UHM-P) and without (UHM) considering porosity change, a for Sample E and b for Sample G

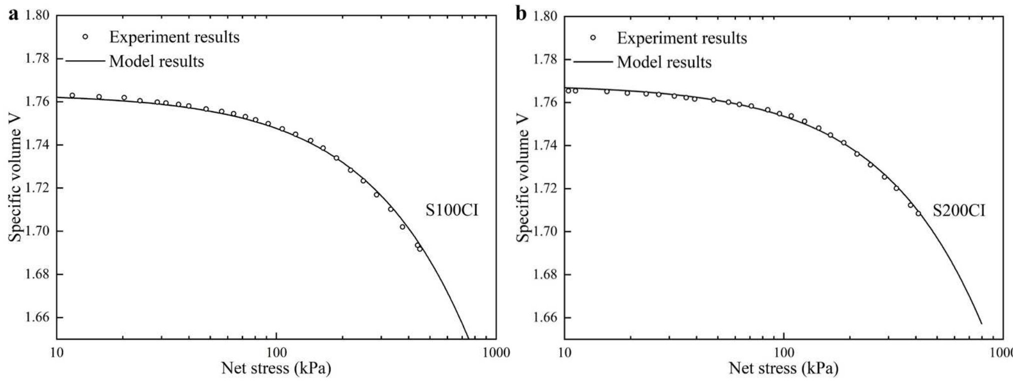

Fig. 8. Comparison of experimental and UHM-P model results for V in Vassallo's test, a for sample S100CI, b for sample S200CI

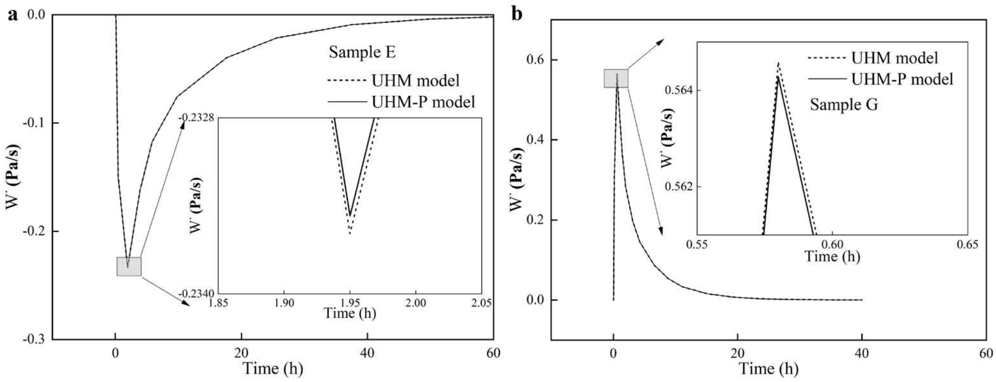

Fig. 9. Deformation energy evolution at the center of samples with and without considering porosity change, a for sample E and b for sample G

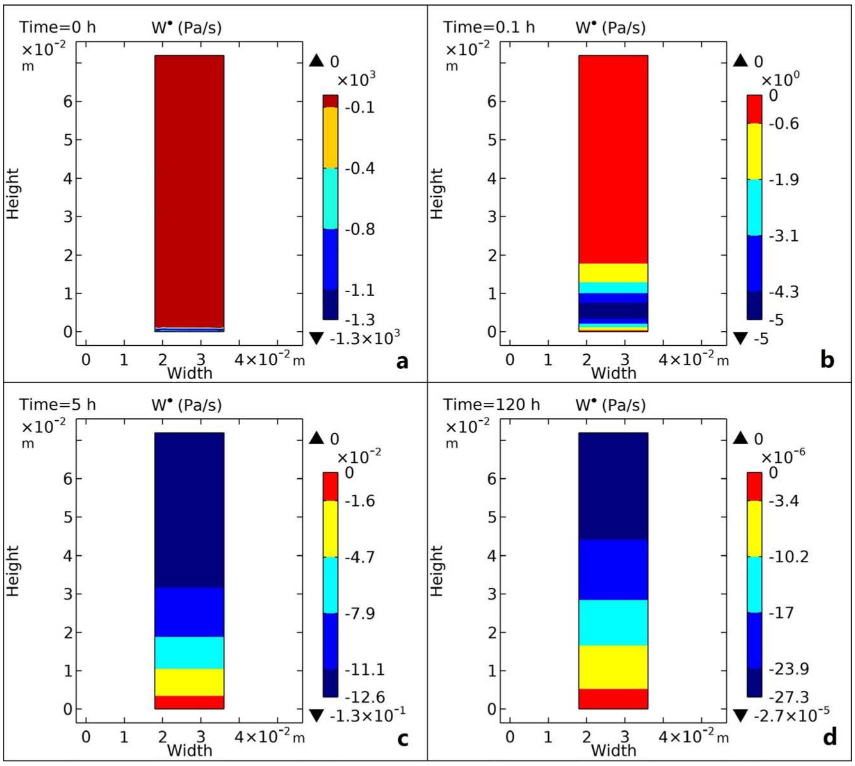

Fig. 10. Deformation energy evolution of sample E with considering porosity change, a for the profile at 0 h, b for 0.1 h, c for 5 h and d for 120 h

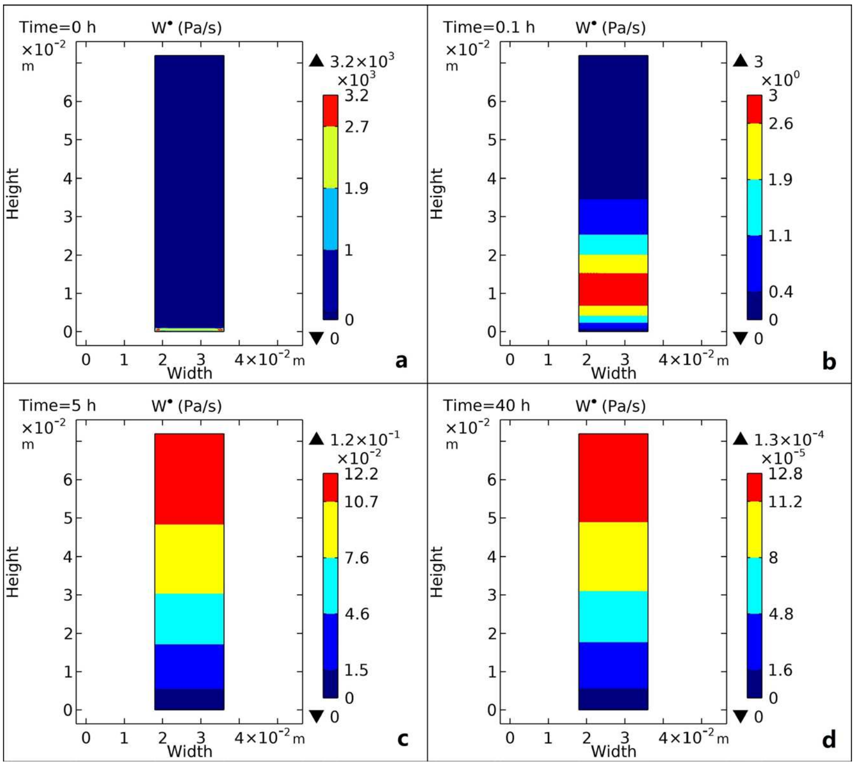

Fig. 11. Deformation energy evolution of sample G with considering porosity change, a for the profile at 0 h, b for 0.1 h, c for 5 h and d for 40 h

Table 1. Hydraulic and mechanical parameters and model setting

Biglari's test	Vassallo's test	Meaning	Parameters
2.428×10^{8} Pa	3×10^{8} Pa	Young's modulus	E
0.214	0.2	Poisson's ratio	θ
2.65×10^{3} $kg\cdot m^{-3}$	2.748×10^{3} $kg\cdot m^{-3}$	Solid density	ρ
5.12 cm	2.485×10^{4} cm	Parameter of Van Genuchten equation	M
1.1459	1.4407	Parameter of Van Genuchten equation	n
8.5×10^{-4} $Pa\cdot s$	8.5×10^{-4} $Pa\cdot s$	Viscosity of water	ν
0.539	0.441	Porosity	υ
1	1	Biot's coefficient	ζ
1.3×10^{-19} m^2	1×10^{-20} m^2	Permeability	k

5×10^{-10} Pa^{-1}	5×10^{-10} Pa^{-1}	Poroelastic storage	q
1.2×10^{2} h	2×10^{4} min	Calculation period	T
0.1 h	10 min	Timestep	Step

Table 2. Parameters used in the sensitivity analysis

Values of different input variation				Parameters
60%	30%	-30%	-60%	
2.08×10^{-19}	1.69×10^{-19}	9.10×10^{-20}	5.20×10^{-20}	$k[m^2]$
8×10^{-10}	6.50×10^{-10}	3.50×10^{-10}	2.00×10^{-10}	$q[Pa^{-1}]$
-	-	0.7	0.4	ζ
3.885×10^{8}	3.156×10^{8}	1.670×10^{8}	9.712×10^{7}	$E[Pa]$

Note: Only 0.4 and 0.7 were evaluated because Biot's coefficient is always <= 1.

Table 3. Error for Δv_w comparing the model to experimental data in Vassallo's test

S100CI	S100P400TG	S100P200TG	S100P100TG	Error estimation
1.0698	0.8631	1.1909	1.3046	$AVRE$
0.9289	0.9028	0.9981	0.9559	R

Table 4. Error for Δv_w comparing the model to experimental data in Biglari's test

G	F	E	D	Error estimation
0.9038	0.9481	1.0985	1.1795	$AVRE$
0.9832	0.9975	0.9963	0.9959	R

Table 5. ROV of each parameter for average volumetric strain

ROV_{min}	ROV_{max}	ROV_{ave}	Variation (%)	Parameter
-0.0332	0.0212	-0.0126	-60	k
-0.0287	0.0176	-0.0077	-30	

-0.0210	0.0134	-0.0042	30	
-0.0188	0.0117	-0.0034	60	
-0.0174	0.0347	0.0056	-60	*q*
-0.0158	0.0287	0.0054	-30	
-0.0125	0.0217	0.0056	30	
-0.0108	0.0193	0.0055	60	
-0.000024	0.00086	0.000094	-60	ζ
-0.000030	0.00087	0.000094	-30	
2.4976	2.5087	2.5015	-60	*E*
1.4242	1.4353	1.4293	-30	
0.7665	0.7718	0.7694	30	
0.6239	0.6266	0.6251	60	

Table 6. ROV **of each parameter for** Δv_w

ROV_{min}	ROV_{max}	ROV_{ave}	Variation (%)	
0.0140	0.5912	0.2272	-60	*k*
0.0030	0.5318	0.1465	-30	
0.0002	0.4601	0.0864	30	
0.0002	0.4286	0.0729	60	
-2.3043	0.0002-	-0.1328	-60	*q*
-1.3140	-0.0002	-0.1162	-30	
-0.7074	-0.0014	-0.1090	30	
-0.5748	-0.0029	-0.1050	60	
0	0.8823	0.0064	-60	ζ
0	0.8839	0.0064	-30	

-1.9291	0	-0.0156	-60	*E*
-1.0990	0	-0.0124	-30	
-0.5907	0	-0.0104	30	
-0.4797	0	-0.0064	60	

Table 7. Error estimation change of Δv_w in samples E and G of Biglari's test with considering porosity change

G(UHM-P)	G(UHM)	E(UHM-P)	E(UHM)	Error estimation
0.9377	0.9038	1.0543	1.0985	*AVRE*
0.9831	0.9832	0.9963	0.9963	*R*